A self-contained, programmable microfluidic cell culture system with real-time microscopy access

Peder Skafte-Pedersen · Mette Hemmingsen · David Sabourin · Felician Stefan Blaga ·
Henrik Bruus · Martin Dufva

Abstract Utilizing microfluidics is a promising way for increasing the throughput and automation of cell biology research. We present a complete self-contained system for automated cell culture and experiments with real-time optical read-out. The system offers a high degree of user-friendliness, stability due to simple construction principles and compactness for integration with standard instruments. Furthermore, the self-contained system is highly portable enabling transfer between work stations such as laminar flow benches, incubators and microscopes. Accommodation of 24 individual inlet channels enables the system to perform parallel, programmable and multiconditional assays on a single chip. A modular approach provides system versatility and allows many different chips to be used dependent upon application. We validate the system's performance by demonstrating on-chip passive switching and mixing by peristaltically driven flows. Applicability for biological assays is demonstrated by on-chip cell culture including on-chip transfection and temporally programmable gene expression.

P. Skafte-Pedersen · M. Hemmingsen · D. Sabourin · H. Bruus ·
M. Dufva (✉)
Department of Micro- and Nanotechnology,
Technical University of Denmark, DTU Nanotech,
Building 345B,
DK-2800 Kongens Lyngby, Denmark
e-mail: martin.dufva@nanotech.dtu.dk

F. S. Blaga
Department of Informatics and Mathematical Modelling,
Technical University of Denmark, DTU Informatics,
Building 321,
DK-2800 Kongens Lyngby, Denmark

1 Introduction

Systems based on microfluidic technology have the potential to be an important future research tool within the cell biology field (Velve-Casquillas et al. 2010; Wu et al. 2010; Yeon and Park 2007; Young and Simmons 2009). Among the advantages of microfluidics compared to conventional technologies are reduced sample consumption, portability, parallelization and increased spatiotemporal control of the sample environment (Liu et al. 2010; Park et al. 2010; Taylor et al. 2009; Velve-Casquillas et al. 2010) leading to possibilities for assays not possible with today's technology. Despite these advantages and the existence of highly advanced systems (Gomez-Sjöberg et al. 2007; Taylor et al. 2009) the microfluidic technology still has not made its entry as a common everyday tool into the biological research laboratories (Whitesides 2011; Young and Beebe 2010; Young and Simmons 2009). In order to fully get the microfluidic technology adopted by the biological society it is time to consider issues such as usability, availability and conformity to existing standards and protocols as pointed out elsewhere (Andersson and van den Berg 2006; Whitesides 2011).

As microfluidic cell culture is still a relatively young field of research, as a natural consequence the development of microfluidic systems has to a high degree been technology driven and focused on implementation and integration of functionality rather than usability and availability.

Often, microfluidic cell culture systems focus only on a subset of components or a single functionality without addressing issues of portability and connectivity to reagents

and actuation hardware. Typical prototyping configurations include a microfluidic chip containing the actual cell culturing and manipulation functions combined with an external perfusion system based on bulk syringe (Hung et al. 2005; Kim et al. 2006; King et al. 2006; Stangegaard et al. 2006) or peristaltic (Wang et al. 2007; Zhang et al. 2009) pumps attached through glued or press fitted needles and extensive tubing. This configuration has advantages in terms of rapid prototyping and device testing without the need for development of pumping solutions. However, bulk pumps heavily restrict system portability and conflict with established working routines, increase required sample volume and limit the number of possible individual inlets to the microfluidic chips. Furthermore, the use of distantly placed pumps connected by extensive amounts of tubing can be prone to formation and trapping of bubbles. Approaches to avoid external pumps include integration of peristaltic pumps on chip using either pneumatic (Hsieh et al. 2009; Kim et al. 2008; Melin and Quake 2007; Yu et al. 2009) or Braille display (Gu et al. 2004; Tung et al. 2007) actuation. This has the advantage of allowing for a large number of pump lines and integration of reservoirs. However, the integrated approach can set restrictions on the possible assays due to a fixed design. Furthermore, actuation of pumps and valves is often still accomplished by large amounts of tubing to external solenoid actuators. Systems allowing for a higher degree of portability have been explored and demonstrated. Examples include a fully portable culturing solution (Futai et al. 2006) and a parallel culturing system with a simple actuation interface by a single pressure source (Sugiura et al. 2008).

Examples of approaches interfacing established standards include a passive culture array by Lindström et al. (2009) containing 672 micro chambers on a chip with dimension of a standard microscope slide. The chip can be seeded by FACS instruments and allows for high-throughput single cell analysis by conventional imaging equipment, but is not constructed for automated perfusion. Systems using the well plate standards include a microbiology fermentation system with easy interconnection and handling by Buchenauer et al. (2009). Lee et al. (2007) presented a 96 well plate based perfusion system optimized for existing equipment and protocols with simple but limited fluid control by gravitationally driven perfusion. Systems for high throughput cell culture have been presented by Meyvantsson et al. (2008) and Puccinelli et al. (2010) combining passive well plate format microfluidics with external pipetting. This allows for a high degree of automation by fluid handling robots.

In this paper we present a stable, self-contained system, which is fully portable and compatible with common working routines of cell biology labs. Based on previously presented interconnection standards (Sabourin et al. 2010a) and improved and further miniaturized near-chip peristaltic micropumps (Skafte-Pedersen et al. 2009) the construction

of the system facilitates handling without specialized skills in microengineering as exemplified by the rapid formation of 32 system-to-chip interconnections formed with only tightening four screws. Yet, it provides up to 24 inlets to one single passive chip and in this and other aspects outperforms other more advanced systems regarding the number of individual fluidic inlet lines (Gomez-Sjöberg et al. 2007; Taylor et al. 2009). The 24 inlets are pumped with three peristaltic micropumps each driving 8 liquid streams. The pumps are programmable in direction and speed over time using custom designed software to provide automated fluid handling. We validate the system by determining switch rate between one reagent and another and mixing in the passive chip. Finally we control and monitor gene expression in living cells.

2 Materials and methods

2.1 System base

The entire system is based on modular components previously described which negate the use for adhesive based permanent assemblies (Sabourin et al. 2010b). With few exceptions all components are custom made in-house by direct mechanical micromilling (Mini-Mill/3, Minitech Machinery Corporation, GA, USA). An overview image of the system with mounted culture medium vials is shown in Fig. 1 and a conceptual system component sketch including peripherals is given in the electronic supplementary material (ESI), (ESI Fig. 1). System components are assembled on a pair of 5 mm thick polycarbonate (PC) base plates. The outer base plate (OBP) rests on the microscope stage and supports the reservoir holders, electrical connector, and inner base plate (IBP). Inlet reservoir holders accommodate up to twenty-four 4 mL glass vials (13090222, La-Pha-Pack GmbH, Germany) with silicone/poly(tetrafluoroethylene) (PTFE) sealed screw caps (13150815, La-Pha-Pack GmbH, Germany) and outlet reservoir holders contain up to six 10 mL glass vials (18091306, La-Pha-Pack GmbH, Germany) with butyl/PTFE sealed screw caps (18031416, La-Pha-Pack GmbH, Germany). The IBP supports three peristaltic micropumps with motors, three inlet adaptors for connecting pumps and reservoirs through tubes, a combined outlet and cell loading block (OCLB) and a support frame for the microfluidic chip (Fig. 2). The IBP is mounted below the OBP in order to fit directly into the central recess of the scanning stage (Scanning stage 130×85 mot; CAN, Carl Zeiss, Germany) for secure mounting by a spring loaded click-on approach. The pumps have integrated, reversibly sealing ball joint interconnections with a self-aligning feature (Sabourin et al. 2010a). The same type of interconnections is integrated in the bottom of the OCLB. These
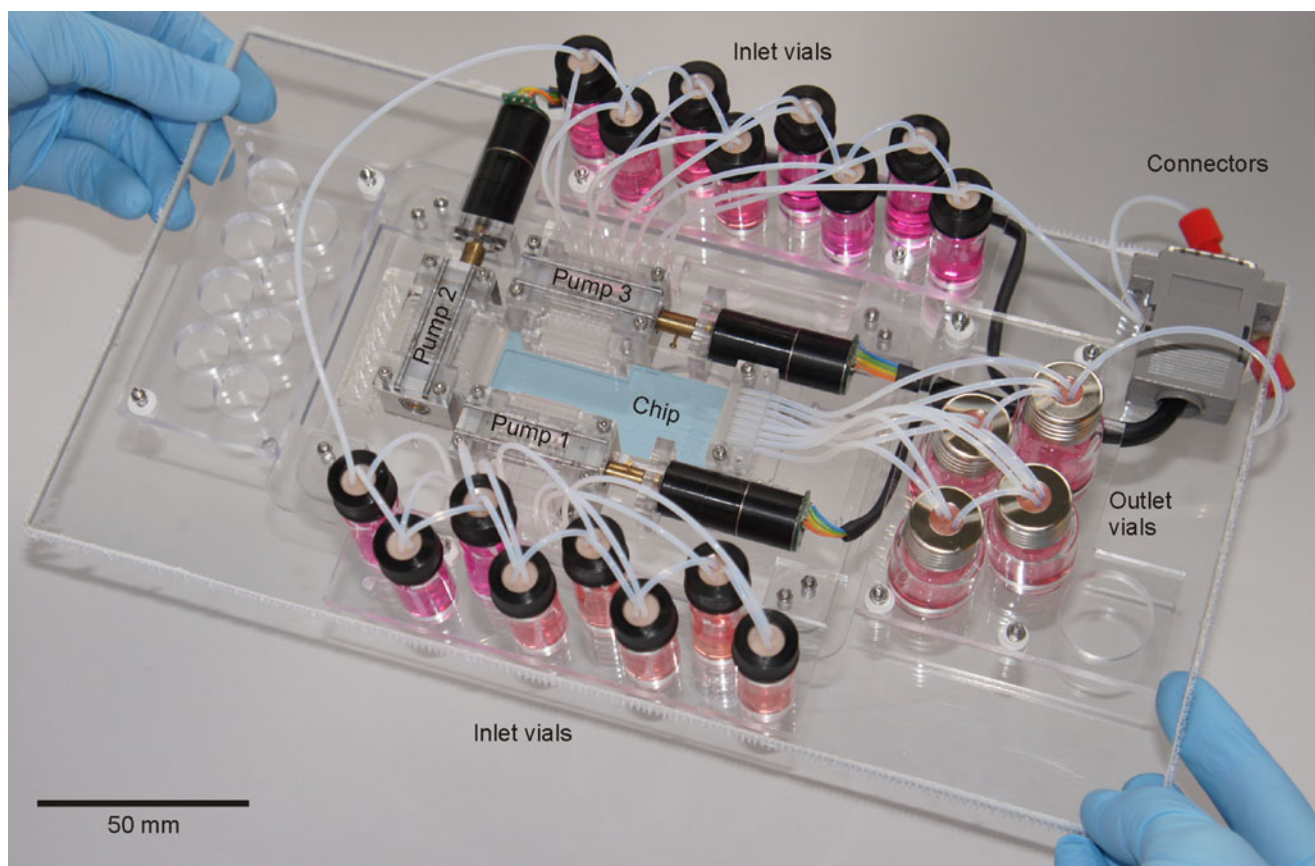
Fig. 1 Complete system including microfluidic chip, 16 inlet vials and 4 outlet vials. Electrical and gas interconnection is seen in upper right corner and the microfluidic chip (highlighted) is attached in the center surrounded by three pumps

integrated ball joint interconnections, which are firmly secured by the IBP are used to interface the microfluidic chips directly to the OCLB and outlet side of the pumps, respectively. The 32 system-to-chip interconnections are established by snapping chips in place and tightening four
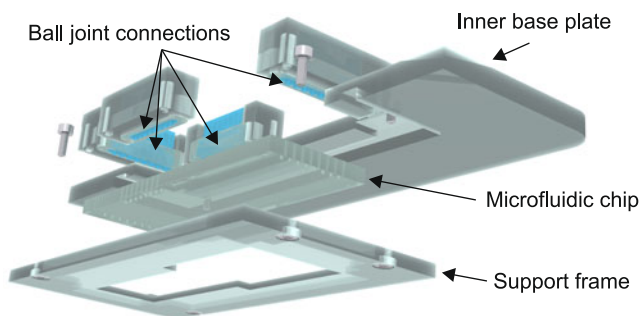

Fig. 2 Exploded view of the interconnection principle for chip mounting. A chip support frame secures and aligns the chip to the inner base plate. The inner base plate supports the 32 ball interconnections, which are directly integrated in the OCLB and pums, respectively. By tightening four screws the 32 interconnections to the chip are established. The inner base plate is cut along the center for visualization and pumps are not shown. The interconnections are visualized by the four blocks each containing eight ball joint interconnections at the bottom side

screws, one in each corner of the chip support frame (Fig. 2). The self-aligning ball joint interconnections and corresponding inlet holes on the chip create interconnections with high sealing strength (Sabourin et al. 2010a). The inlet sides of the pumps have mounted inlet adaptors containing cylindrical cavities with a volume of ~30 μL. These can be used either directly as pipetting reservoirs for short assays or a connection base for connecting the pumps to the glass vials *via* PTFE tubing. In the latter case a piece of silicone tubing (1×3 mm, 228–0701, VWR, Belgium) is mounted in the hole to serve as a gasket for PTFE tubing (BOLA 1810–01, Bohlender GmbH, Germany). The outlet block is a combined structure of PC and poly(dimethylsiloxane) (PDMS) containing eight integrated ball joint interconnections and eight ~15 μL chambers, which serve as both socket for PTFE outlet tubing and reservoirs for loading up to eight different cell suspensions.

The entire system is enclosed in an incubator (Incubator XL Dark S1, Carl Zeiss, Germany) when mounted in the microscope. To limit the influence of gas permeable materials on the liquid the entire system is equipped with a flexible atmosphere cover during long-term cell culture. The cover is reversibly attached by Velcro® tape and fed with a

humidified CO_2 enriched gas mixture (CO_2 module S1, Carl Zeiss, Germany).

2.2 Chip design and fabrication

The employed microfluidic chips are based on PMMA (Plexiglas XT 20070, Röhm GmbH, Germany and Solaris Clear S000, PSC A/S, Denmark) and fabricated by micro-milling followed by a UV assisted local heat bonding (Truckenmüller et al. 2004). In short, the individual layers of the chip were cleaned with 70% EtOH and Milli-Q water before being exposed to UV (DYMAX, 5000 EC with bulb 36970, CT, USA) for 90 s. Following exposure the layers were sandwiched between two glass slides in an alignment setup and bonded for 20 min at an initial bonding pressure of 2.3 MPa in a laboratory press (PW 10 H, P/O/Weber, Germany) pre-heated to 85°C. All chips have a total thickness of 3.5 mm and are, depending on the specific design, composed of individual sheets of PMMA ranging from 0.5 mm to 2 mm in thickness. The bottom layer of all chips is 0.5 mm for reduced optical path length from the sample to the objective. A total of 32 fluidic inlets and outlets are implemented as 800 μm holes in the top of the chip. Inlets are spaced 2.25 mm apart to conform with 1,536 microtiter well plate standards and placed along each chip side in groups of 8 to interface pumps and OCLB. The chip for cell culture and programmable gene expression (Fig. 3(a)) contains eight parallel fluidic networks each having three inlets meeting in a common intersection upstream a mixer and culturing chamber. The chamber has a footprint of 1.5 mm width by 4 mm length capped by isosceles triangles. Chamber height is 500 μm and inlet and outlet channels are connected at the top surface of the chamber.

Characterization of switching and mixing of liquids is made with chips containing four T-junctions with inlets routed from either the same or two neighboring pumps in order to test different flow combinations (Fig. 3(b)). Each mixer has an outlet channel length of 88 mm and a cross sectional area of 400 μm width and 150 μm height. Since the diffusive leak is dependent on the fluid velocity and thus intersection geometry the influence of geometry is tested through two variants of the intersection, one with 400 μm by 150 μm intersection and another with a constricted 200 μm by 70 μm intersection. 3D images of these can be found in ESI Fig. 2.

2.3 Pump construction

The pump construction is an upgraded and further miniaturized version of a previously presented work (Skafte-Pedersen et al. 2009) based on the three central components highlighted in Fig. 4. A peristaltic multi roller (MR) consisting of a central brass drive shaft encircled by eight stainless steel pins secured in nylon holders and connected to ball bearing end
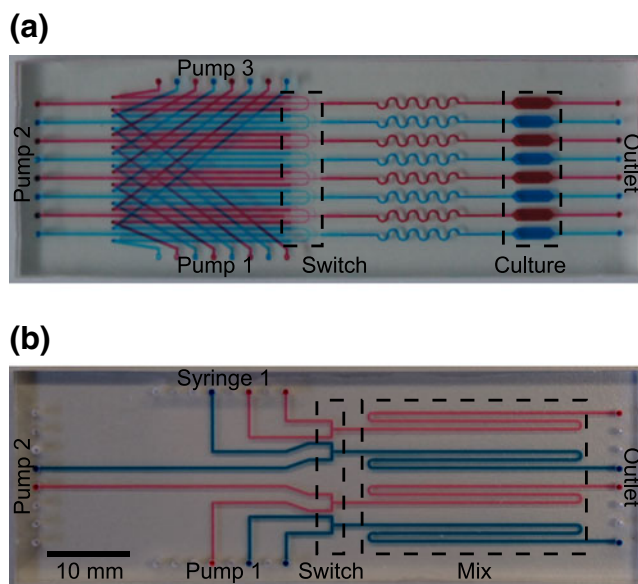

(a)

(b)

Fig. 3 (a) Photo of programmable cell culture chip running 8 parallel assays. Three sets of inlets are each coupled to a pump and combined on the chip in a passive T-junction. Each of the 24 inlets can contain a unique compound although actuation is coupled in groups of 8. An intermediate passive mixing section ensures homogeneous sample exposure in the downstream cell culturing chambers. (b) Photo of characterization chip containing four different T-junctions for investigating peristaltic switching and mixing with different combinations of peristaltic pumps and syringe pumps. Red and blue food coloring is used for visualization of the individual fluidic networks

pieces occludes a monolithic PDMS microfluidic ribbon (μFR) with eight integrated channels against a static, supporting rotor bed (RB). The μFR is bookended by handling pieces in PMMA and integrated ball-joint interconnections for direct chip attachment.

The footprint of the central pump elements, including two sections for fluidic interconnections of all eight channels is 30×40 mm^2 and the total height is 20 mm excluding bolt heads. By rotating the MR, fluid volumes occluded between two pins are transported through the integrated tubing in the direction determined by the rotation of the MR. Due to a symmetric construction of the pumps their action is bidirectional with the same flow characteristics in either direction. A detailed description of pump operating principles is provided in Skafte-Pedersen et al. (2009).

For perfusion flow rates on the order of 100 nL min^{-1} per fluidic channel low rotational speeds on the order of 10^{-1} min^{-1} are required. To achieve a smooth motion at such low speeds combined with a minimum footprint and weight for microscopy compatibility a geared stepper motor is used. The chosen model, which has a cross sectional area smaller than the remaining pump parts, is a 24 step miniature stepper motor (PRECIstep AM 1524, Faulhaber, Germany) equipped with a planetary precision gearhead of reduction ratio 152:1 (15A, Faulhaber, Germany). Including motor and
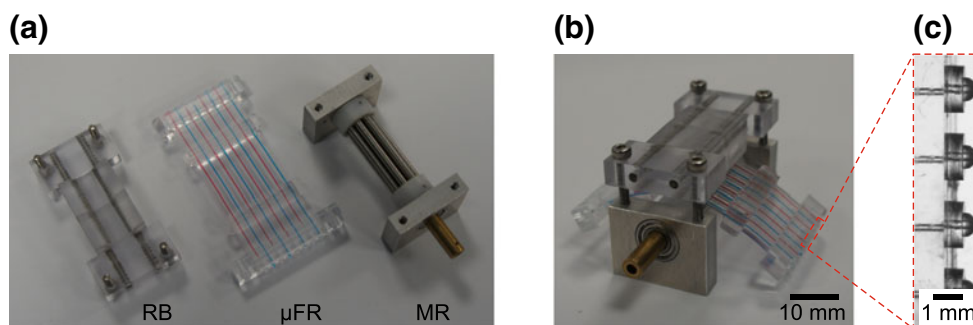
gearhead the total length of a complete eight-channel pump is 100 mm and the mass limited to approximately 50 g.

2.4 Peripheral components

A custom built control box powered by an external power supply (KY-05036S-12, Leadman Electronic Company, Inc., Taiwan) contains three stepper motor circuits (Stepper Motor Driver TA8435HQ CNC, Markus Mechatronics, Germany) and a USB I/O card (LabJack UE9, LabJack Corporation, CO, USA) as the main components. The system is connected to the control box through 12 electrical phases in a single ribbon cable terminated by a standard multipin connector. For long term cell culture the inlet and outlet reservoir caps are coupled with PTFE tubing (BOLA 1810–10, Bohlender GmbH, Germany) and pressurized with an air and 5% CO_2 mixture through a sterile filter with a single Luer-Lok fitting.

2.5 Software control

The fluidic actuation is controlled by custom-built software based on Visual Basic for Applications (VBA) for direct integration of the pump control in the AxioVision microscopy software (AxioVision 4.8.2, Carl Zeiss, Germany). For advanced long term assays such as temporal cell programming requiring changes in perfusion settings over time, a module integrating each pump setting with a corresponding acquisition and automated image analysis sequence has been developed. The module is fed with an external MS Excel file containing the predefined perfusion, acquisition and analysis settings for each phase of the experiment. A simpler software version containing only pump control without pre-programmed sequences has been implemented directly in Excel. All data in this article has been produced using the latter software version.

2.6 Numerical mixing model

Numerical finite element method (FEM) simulations are implemented in Comsol (Comsol 3.5, Comsol AB, Sweden).

A 2D FEM model combining an incompressible Navier–Stokes model with a convection-diffusion model in steady state is made for determination of steady state mixing. The Navier–Stokes model includes a volume force to account for the top and bottom surface of the channel identical to the built in Comsol shallow-channel approximation. The geometry is restricted to include the first 2 mm of the inlet channels and 56.5 mm of the outlet channel.

Boundary conditions (BC) for the Navier–Stokes model are normal inflow velocity at inlets, pressure with no viscous stress at the outlet and a no-slip condition at side walls. BCs for the convection-diffusion model are fixed concentration at inlets, convective flux at outlet and no-flux symmetry conditions at side walls. Concentration data are extracted for further processing from 360 µm long cross sectional plots sampled with a distance of 0.5 mm along the channel.

2.7 Analytical diffusive leak model

Due to the valveless construction of the chips there will be an inherent diffusive leak from the intersection when one or more inlets are stopped. An analytical 1D model based on the steady-state convection-diffusion equation combined with a characteristic diffusion time and length relation has been developed for design guidelines. If we assume a stagnant inlet channel to hold a solute with diffusion coefficient D and concentration c_1 connected to an infinite upstream reservoir of concentration c_1 we can find the diffusive leakage concentration c_B in the outlet channel subject to an average fluid velocity v_1. A constant concentration BC at the inlet combined with continuity in concentration and convective-diffusive flux at the intersection and a downstream pure convective flux at the outlet is employed to develop a steady state model. Combining this with the characteristic diffusion length $l = \sqrt{2Dt}$ results in the following time-dependent estimate for the leak concentration expressed in terms of the characteristic leak ratio χ

$$\chi \equiv \frac{c_B}{c_1} = \frac{D}{D + v_1\sqrt{2Dt}}. \tag{1}$$

Using this as a design parameter it is clear that the diffusive leakage can be limited by increased velocity at the intersection and increased time. However, it should be noticed that the estimate is only valid for $\sqrt{2Dt} \leq x_1$, where x_1 is the distance from the intersection to the infinite reservoir.

Due to diffusion between the intersection and stagnant channel there will be a time lag when switching pump settings due to required flush of the contaminated stagnant channel. Assuming the intersection to be a constant source this lag can be estimated by the volume V_p contaminated during stagnant conditions over time t_s from the characteristic diffusion length $l_p = \sqrt{2Dt_s}$. Based on this, the lag time t_l required to flush the contaminated volume V_p can be estimated to be

$$t_l = whQ^{-1}\sqrt{2Dt_s}. \tag{2}$$

More in-depth derivations can be found in the ESI.

2.8 Numerical time-dependent switching model

2D FEM models are employed to determine the time dependence of the switching in a T-junction including the initial convection flushing phase and subsequent convection-diffusion balance leading towards a steady state leak. The models are implemented by a coupled steady-state Navier–Stokes and time-dependent convection-diffusion application mode. The model includes a volume force to take viscous stress from the top and bottom of the channel into account as used in the mixing models as well. For the model shown in Fig. 5 we use the following boundary conditions for the convection-diffusion equation: Inlet A has a constant concentration of unity representing an infinite reservoir and inlet B concentration of zero as the concentration of the flushing liquid. At the outlet the flux is assumed purely convective. All other boundaries are symmetry conditions. For the Navier–Stokes model, inlet B has a parabolic inlet
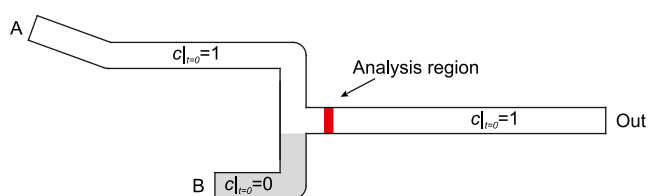

Fig. 5 Overview of initial and boundary conditions for numerical FEM model. Initial conditions in concentration are $c=1$ and $c=0$ in the white and grey areas, respectively. Boundary A has a constant concentration condition and the outlet is assumed convective flux in the convection-diffusion model. Inlet B has a constant inlet velocity and the outlet a no stress condition in the Navier–Stokes model. Area used for numerical analysis of average leak downstream the intersection is highlighted

velocity dependent on the flow rate. The outlet is a pressure outlet condition with no shear stress. All other boundaries are no-slip conditions.

As initial condition the upper inlet channel and the outlet channel are maintained at concentration $c=1$, whereas the lower inlet channel is at $c=0$ as illustrated in Fig. 5. The model containing a constricted junction assumes a constant channel height of 70 μm in the entire domain, since the switching dynamics are dominated by the convection-diffusion balance in the intersection. The convection-diffusion model is solved with a time dependent solver at time steps of 1 or 4 s for flow rates of 1,000 nL min^{-1} or 250 nL min^{-1}, respectively.

2.9 Flow characterization

Flow patterns and characteristics of a separate pump as well as on-chip convection-diffusion dynamics were determined. For time-dependent flow pattern determination the outlet from individual channels of a peristaltic micropump were connected to a thermal anemometry volume flow sensor (Flowell, Fluigent, France) by PTFE and polyetheretherketone (PEEK™) tubing (BOLA 1810–10, Bohlender, GmbH, Germany and Upchurch Scientific 1581, IDEX Health and Science, WA, USA) via an intermediate PMMA tubing connector chip. The inlet side of the pump was connected by PTFE to an open reservoir containing Milli-Q water by PTFE tubing and connector chip. Custom made software in Matlab R2010a (The MathWorks, MA, USA) was used to plot the pattern.

Determination of channel-to-channel and pump-to-pump variability were made in a separate test setup containing a chip with sixteen 1×1 mm^2 channels addressed by two individual micropumps, where the advancing fronts of a water-based dye solution were used to determine pumped volume per full pump rotation. For this purpose and for durability tests another motor type (LEGO® Mindstorms®, Denmark) with higher rotational speed capabilities was used.

For on-chip characterization of switching rate and mixing capabilities using the chip shown in Fig. 3(b) the inlets in each T-junction were discriminated by feeding one inlet with a combined fluorescent and absorbing solution and the other inlet with an absorbing solution. For matched absorbance and excitation wavelengths this technique eliminates signal from the upper part of the channel by Lambert-Beer absorption as described by Bancaud et al. (2005). Fluorescein sodium salt (FS) (Sigma 46960-25 G-F) was used as fluorescent dye and Orange G (OG) (Sigma O3756-25 G) was employed as a matching absorbing dye. Concentrations of $c_{FS}=1$ mM and $c_{OG}=30$ mM were used to obtain the best compromise between fluorescent signal and decay length based on a parametric scan of concentration

combinations (unpublished results). The two dyes were dissolved in a 50 mM carbonate-bicarbonate buffer solution (CBB) (Sigma C-3041) with a nominal pH of 9.6. As the nonfluorescent absorbing solution a 30 mM OG solution in 50 mM CBB was used to ensure identical absorption characteristics over the entire channel width. Based on the theory presented by Bancaud et al. (2005) this gives a 95% intensity reduction over 24 μm with the employed Zeiss EC Plan-Neofluar 10×/0.3 Ph1 objective.

The fluids for peristaltic pumping were contained in 4 mL glass vials connected by PTFE tubing (BOLA 1810–01, Bohlender GmbH, Germany) and the chip outlets were connected to 5 mL glass vials through PTFE tubing. Image acquisition software was AxioVision and automated analysis was performed by custom made software in Matlab with the aid of Bio-Formats (LOCI, UW-Madison, WI, USA) for reading the Zeiss ZVI file format.

2.10 Switching

For switching characterization a single T-junction was attached to two independent peristaltic pumps. The switching efficiency was evaluated by switching off the fluorescent inlet and turning on the nonfluorescent. Two different flow rates of 250 nL min⁻¹ and 1,000 nL min⁻¹ were used. Prior to switching, the system had been running at the initial condition for a minimum of 2 or 8 min at 1,000 nL min⁻¹ or 250 nL min⁻¹, respectively. The flow rates denote average flow rates.

Time-lapse series with a temporal distance of 2 s or 8 s at 1,000 nL min⁻¹ or 250 nL min⁻¹, respectively, were recorded using a 10×/0.3 Plan-Neofluar objective, 62HE filter, 470 nm Colibri LED light source and a Zeiss Axio-Cam MRm B/W camera. First image was acquired approximately 1 s before change of pump settings to ensure recording of initial condition. For each geometry and flow rate combination a total of three repetitions were made. Fluorescent images were background corrected by a pixel-to-pixel subtraction of background images recorded with a pure OG flow before and after the measurement series. The fluorescent signal was quantified by calculating the densitometric mean based on the individual pixel values in a 125 μm wide stripe centered 750 μm downstream the rear edge of the intersection. The values were normalized to the densitometric mean of the first frame in each measurement series. The mean and standard deviation for each setting was calculated and plotted against a time scale, which was shifted 1 s to account for delay between start acquisition and change of pump settings. Conversion from intensity to fluorophore concentration was done by a 1:1 correlation based on a standard curve (data not shown).

2.11 Mixing

For determination of mixing properties the four T-junctions of the chip given in Fig. 3(b) were connected to the nonfluorescent OG and fluorescent FS/OG mixture. The schematic representation for each junction can be found in ESI Fig. 3.

To compare the mixing from pulsating peristaltic pumps to steady flow from syringe pumps a number of combinations were made. Junction A was fed by a single peristaltic pump in phase, junction B was connected to two peristaltic pumps with arbitrary phase shift, junction C was connected to a peristaltic pump and a syringe pump (CMA 400, CMA Microdialysis, Sweden) equipped with 1 mL syringes (BD Luer-Lok Tip 1 mL, ref 309628, Becton, Dickinson and Company, NJ, USA) and junction D was operated by the same syringe pump. The nominal, average flow rate ratios of the inlets were 1:1 in all four junctions and the total flow rate was 250 nL min⁻¹ or 1,000 nL min⁻¹ per junction, respectively.

Image acquisition was performed using the same equipment as for switching experiments but measured at positions 0, 2, 4, 8, 16, 32 and 48 mm downstream the front edge of the intersection in order to determine the diffusive mixing as function of convection distance. At each position, a 20 s time-lapse series with 2 s intervals was acquired and repeated 2×3 times per setting for a total of 66 images in both bright-field and fluorescence per position per flow rate setting.

Mixing efficiency was quantified by the mixing index M as given by Lee et al. (2000). If we introduce the average pixel intensity I and the standard deviation of the sample σ_s on the pixel intensity the mixing index can be expressed as

$$M = 1 - \frac{\sigma_s}{\overline{I}}. \qquad (3)$$

The fluorescence images were used for statistical evaluation of the mixing index along a line across the channel. Optical edge effects were eliminated by centering and limiting the analysis segment to 360 μm and a manually determined background pixel value based on analysis of an OG filled channel was subtracted and the line segment smoothed before calculation of the mixing index for each individual image. Subsequently, the mean and standard deviation of the mixing index at each position and condition were calculated and plotted against the distance from the junction.

2.12 Cells and culture medium

HeLa Tet-On® Advanced cells (631155, Clontech) were cultured in DMEM/F-12 + GlutaMax™ (31331, GIBCO) supplemented with 10% Tet System Approved Fetal Bovine Serum (FBS) (631106, Clontech), penicillin 100 U mL⁻¹, streptomycin 100 μg mL⁻¹ (P4333, Sigma), and geneticin

(G-418) 100 µg mL^{-1} (11811–023, GIBCO). At conventional cell culturing the cell line was incubated at 37°C and 5% CO_2.

2.13 Microfluidic cell culture

Liquid glass vials, caps, and PTFE tubing were sterilized by autoclaving before use. Glass vials, tubing and connections to pumps were assembled onto the system base plate. The cell culture chip and tubes connecting the liquid reservoirs to the pumps were filled separately with Milli-Q water to remove bubbles, before clicking on the cell culture chip to the IBP. Inlet and outlet reservoirs were coupled with PTFE tubing (BOLA 1810–10, Bohlender GmbH, Germany) and supplied with air supplemented with 5% CO_2 through a sterile filter. To avoid formation of gas bubbles a pressure of 0.3 bar was put on the flow system during the whole system preparation and cell culture period, only interrupted when for instance changing liquid reservoirs.

The connected flow system was sterilized by flushing with 0.5 M NaOH for 20 min at a flow rate of 4.5 µL min^{-1}, followed by washing with sterile water for 30 min at a flow rate of 4.5 µL min^{-1} to remove all NaOH. The surface of the cell culture chambers was coated by passing a 50 µg mL^{-1} polyethyleneimine (PEI) (408727, Sigma) solution in phosphate buffered saline (PBS) through the chip at a flow rate of 4.5 µL min^{-1} for 15 min followed by 195 nL min^{-1} for 1.5 h at room temperature. After coating, the flow system was flushed with cell culture medium for 20 min at a flow rate of 4.5 µL min^{-1} before cell loading. Prior to cell loading the outlet tubes were removed from the OCLB.

HeLa Tet-On® Advanced cells were resuspended in cell culture medium added 0.025% w/v collagen (Sigma C3867) before about 10 µL suspension of a cell density of 5×10^5 cells mL^{-1}, corresponding to a surface density of 250 cells mm^{-2}, was loaded into embedded wells in the OCLB in a LAF bench. The system was transferred to the microscope and cells were introduced into the cell culture chambers by setting the pumps to run backwards at a flow rate of 4.5 µL min^{-1} for about 1 min. Afterwards, the outlet tubing and reservoirs were attached to the OCLB under sterile conditions in a LAF bench. The system was equipped with the atmosphere cover and clicked onto the microscope stage before reconnected to CO_2, pressure and electrical supplies. The system was incubated in an atmosphere setting of 37°C and 8% CO_2 to keep a pH of the cell culture medium at about 7.0–7.2. After cell loading, the cells were left without flow for 2 h, and then perfused with a low flow rate of 33 nL min^{-1} for another 2 h. Following this attachment phase, the HeLa Tet-On® Advanced cells were perfused at a flow rate of 500 nL min^{-1} until completion of the experiment.

2.14 Regulated fluorescent reporter gene expression

DD-ZsGreen1-DR was cut out from pZsGreen1-DR (632428, Clontech) and cloned in-frame with the DD tag sequence in the multiple cloning site in pTRE-Cycle2 (631116, Clontech). Plasmid amplification was carried out in One Shot® TOP10 Chemically Competent E. coli (C4040, Invitrogen) cultured either in LB Broth (L7275, Sigma) or on LB agar (L7025, Sigma) added Kanamycin 50 µg mL^{-1} (K1377, Sigma) or Ampicillin 100 µg mL^{-1} (171254, Calbiochem). The plasmids were purified by using PureLink™ HiPure Plasmid DNA Purification Kit (K2100, Invitrogen) and diluted in TE-buffer to 100 ng mL^{-1}. HeLa Tet-On® Advanced cells passage 10 were loaded into the cell culture chambers on chip as described above. After 20 h of cell culturing and at a cell confluence of approximately 80%, the cells were transfected on chip. Briefly, 6.25 µg plasmid DNA (pTRE-Cycle2-ZsGreen1-DR) was diluted in 2.5 mL OptiMem medium (31985, GIBCO) and added 15.6 µL of Lipofectamine™ LTX (15338–100, Invitrogen) giving a proportion of DNA to Lipofectamine of 1:5. After gently mixing and incubation at room temperature for 25 min, the transfection complexes were diluted 1:3.2 in cell culture medium and then flushed into the cell culture chambers at a flow rate of 1.0 µL min^{-1} for 20 min. The transfection process was performed without flow for 60 min, followed by a short flow period at a flow rate of 0.5 µL min^{-1} for 10 min. These two steps were repeated for 6 h in total. Finally, the transfection complexes were removed by flushing with cell culture medium at a flow rate of 1.0 µL min^{-1} for 20 min. Cell culture was continued at a flow rate of 0.5 µL min^{-1} for another 18 h, before inducing mCherry and DD-ZsGreen1-DR gene expression by switching to cell culture medium supplemented with doxycycline 0.5 µg mL^{-1}. DD-ZsGreen1-DR was stabilized by another switch to medium added doxycycline 0.5 µg mL^{-1} and Shield1 0.5 µM and perfusion with doxycycline and Shield1 was continued for another 21 h. Lastly, a final switch was made to medium with doxycycline but without Shield1. Cell culture was continued for an additional 19 h before completion of the experiment.

2.15 Imaging and image analysis

Time-lapse series of regulated fluorescent reporter gene expression were recorded every hour by a Zeiss Axio Observer.Z1 microscope equipped with a 10×/0.3 Plan-Neofluar objective, Colibri LED light source and a Zeiss Axiocam MRm B/W camera. A scan of 6×2 images, all acquired with a z-stack of seven slices (5 µm between each slice), were recorded for each chamber. The DD-ZsGreen1-DR signal was acquired at 470 nm excitation wave length through a 62HE filter, while mCherry was excited at 555 nm

and emission light acquired through a 43HE filter. DD-ZsGreen1-DR was exposed for 10 ms and mCherry for 500 ms. The images were processed by stitching the individual images together, converting the stitched images to one image and finally applying the AxioVision Extended Focus module on the z-stacks to obtain the best focused image. The fluorescent signal was quantified by calculating the densitometric sum (DS) based on the individual pixel values of the converted 16 bit image in the range between 1000 and 62955 for DD-ZsGreen1-DR and 1032–62439 for mCherry. Mean value of densitometric sum based on six individual chambers was calculated and normalized to the highest recorded value. The normalized averages and normalized standard error on the mean (SEM) for the regulated DD-ZsGreen-DR were plotted as function of time.

3 Results

3.1 System

The presented system is self-contained, modular and optimized for programmable long-term cell culture on microscope stages. The system is based on three peristaltic micropumps and a number of self-aligning interconnections (Sabourin et al. 2010a; Skafte-Pedersen et al. 2009). The central part of the system is an exchangeable cell culture chip equipped with 32 holes for fluidic input/output (I/O). Ball joint interconnections allowed the central microfluidic chip to be attached directly to 32 fluidic lines with a simple snap-on approach by securing four bolts between the chip support frame and the inner base plate. The system base plate is capable of holding up to 24 autoclaveable inlet reservoirs providing sufficient liquid for 5–10 days of cell culture and stimulation under typical conditions. With the exception of external pressure and power supply, which are attached via two standard connectors, all components and reagents are securely mounted and enclosed on a single, portable base, cf. Figure 1. Moving the system between workstation such as LAF benches, incubators and microscopes only required that the pressure source and the pump control cable were disconnected from the base plate. Disconnection and reconnection of the pressure source and control cable takes less than 1 min to perform. Because the fluidic connection from inlet vials to outlet vials *via* pumps and chip is not broken during disconnection of external control and pressure cables, this operation entails no risk of introducing bubbles during transport between work stations.

The base plate design with a lowered IBP ensured that the system was securely mounted in the microscope stage for long-term, multi position microscopy. The lowered IBP also allowed for use of objectives with low to medium working distance (WD). The compact size of the pumps combined with the direct chip attachment allowed the pumps and chip to fit between the condenser and objective of standard life science inverted microscopes. The current system is optimized for a motorized, inverted microscope (Zeiss Axio Observer.Z1, Carl Zeiss, Germany) with a motorized condenser with WD of 26 mm and objectives with a WD down to 2.5 mm.

3.2 Flow characteristics

The pumps are based on peristaltic occlusion of confined fluid volumes between the multi-roller pins and are therefore inherently pulsatile. Figure 6 shows an example of the flow pattern at an average flow rate of 0.36 µL min^{-1}. A distinct pulse pattern with typical pulse volumes of 0.08 µL is seen. Two pumps were tested to have average displaced volumes per full MR revolution ranging between 0.64 µL and 0.74 µL per revolution. The relative standard deviation in displaced volume between channels in individual pumps was tested to be between 2.8% and 8.7% similar to values for the previously reported pump (Skafte-Pedersen et al. 2009). Durability tests of the pumps were voluntarily stopped after 63,000 full revolutions. Using the minimum measured channel volume of 0.52 µL per revolution this corresponds to a pumped volume of approximately 33 mL per channel. For a typical culture experiment with average flow rates of 0.5 µL min^{-1}, the pumped volume corresponds to more than 45 days of continuous culture.

3.3 Switching

The system operates with passive chips, i.e. chips not containing any movable parts, and three pumps that each function as a closed valve when stopped. This means that liquid could be switched using T-junctions on the chip by stopping one pump and starting another. Since the chip did not contain a valve at the merging point of the liquid streams, it was necessary to determine the amount of diffusive leak from the stopped liquid line into the downstream line. Effects of switching were investigated for two flow rates
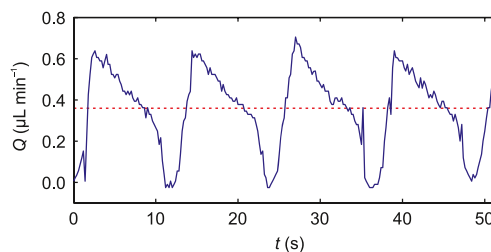

Fig. 6 Excerpt of peristaltic pump pattern showing flow rate Q vs. time t at an average flow rate of 0.36 µL min^{-1} measured with a thermal anemometry flow sensor. Typical pulse volumes are 0.08 µL. The dashed line indicates the average flow rate

Table 1 Time t to reach 1% and 0.1% diffusive leak ratio χ. Two different flow rates and intersection designs are used. For numerical modeling the reservoir to intersection distance is 5 mm and diffusion coefficient 6×10^{-10} m^2 s^{-1}

	Q (nL min^{-1})	Small intersection		Larger intersection	
		$t_{1\%}$ (s)	$t_{0.1\%}$ (s)	$t_{1\%}$ (s)	$t_{0.1\%}$ (s)
Experimental	250	3.9×10^1	N/A	4.3×10^2	N/A
Numerical	250	4.0×10^1	N/A	6.4×10^2	N/A
Analytical	250	3.3×10^1	3.4×10^3	6.1×10^2	6.2×10^4
Experimental	1000	1.5×10^1	N/A	0.9×10^2	N/A
Numerical	1000	0.8×10^1	2.3×10^2	0.9×10^2	N/A
Analytical	1000	0.2×10^1	2.1×10^2	0.4×10^2	3.9×10^3

(Table 1) and geometries at the merging point (ESI Fig. 2). The experimental, numerical and analytical results of the passive on-chip switching are summarized in Figure 7. The diffusive leak ratio decreased more rapidly for the high flow rate than low flow rate for each cross section geometry and more rapidly for merging point with constricted cross section compared to large cross section. The finite bit depth of the employed camera (12 bit) and correction for a background, which changes slightly over the course of an experiment, put a limit on the possible resolution of the measured leak ratio. For this reason, only data points down to leak ratios of 1% have been included. 1% was arbitrarily decided to have no or little biological effect. At high flow rate and with the constricted cross section, the 1% leak was reached after about 15 s. For high flow rate and large volume cross section, 1% diffusive leak was reached after about 90 s. For lower flow rate the 1% diffusive leak ratios
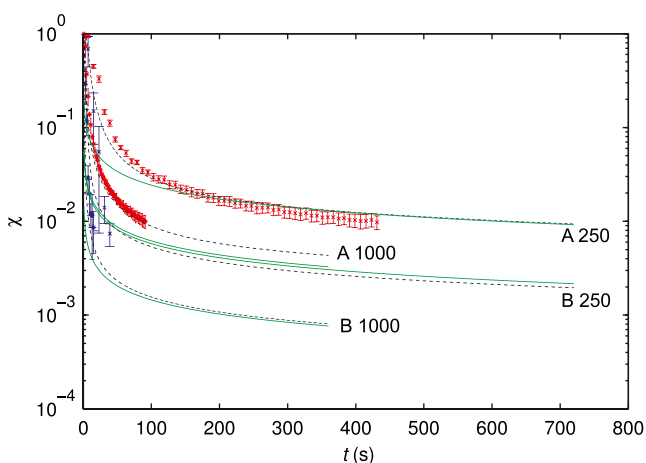

Fig. 7 Experimental, numerical and analytical result for the leak ratio χ vs. time t, cf. Eq. (1), during passive on-chip switching in T-junctions with and without constriction. Experiments A correspond to the largest intersection and B to the smaller, constricted intersection, cf. ESI Fig. 2. Annotations 250 and 1,000 refer to the flow rate in nL min^{-1}. Experimental data are averaged values ± standard deviation. Dashed lines represent numerical results and solid lines the corresponding analytical estimates. A diffusion coefficient of D=6×10^{-10} m^2 s^{-1} both analytical and numerical models and a stagnant channel length of 5×10^{-3} m was used for numerical modeling

were observed after 0.7 and 7.2 min for constricted and large volume cross sections, respectively. Diffusive leak was determined by analytical and numerical models using a diffusion coefficient of D=6×10^{-10} m^2 s^{-1} and a stagnant channel length of 5×10^{-3} m. Diffusion coefficient value is based on data from Rani et al. (2005) scaled with temperature through the Stokes-Einstein relation. Table 1 summarizes the times for reaching 1% and 0.1% leak ratios based experiments and analytical and numerical models using the same modeling parameters as in Fig. 5. The analytical model uses the average fluid velocity based on flow rate and channel cross section. For all four combinations of geometry and flow rate a fair correlation between experiments and numerical and analytical models is observed.

Lag time due to upstream diffusive contamination after long-term stagnancy in the stopped inlet channel has also been estimated. The characteristic lag times t_l for flushing the inlet channel after long-term stagnancy was calculated from Eq. 2. With typical system values (D=6×10^{-10} m^2 s^{-1}, w=400 μm, h=150 μm) the affected volume after 24 h is 0.6 μL. Assuming a typical flow rate at switching of 0.25 μL min^{-1}, the corresponding lag time t_l for clearing the previously stagnant inlet channel is approximately 2.4 min.

3.4 Mixing

The effect of pumping mechanism on mixing efficiency was investigated using different combinations of pump possibilities (ESI Fig. 3). Mixing of pulsatile flow (peristaltic micropumps), steady flow (syringe pump) and combination thereof was compared (Fig. 8). There was no difference of practical importance in mixing between steady state flows and peristaltically induced oscillating flows. We also found a fair correlation between measurements and numerical results based on steady state flow (Fig. 8). The same overall tendency for mixing with peristaltic pumping were obtained for flow rates of 0.25 μL min^{-1} (data not shown) and 1.0 μL min^{-1} (Fig. 8). These results indicate that the peristaltic micropumps essentially perform equal as pumps generating steady flow in terms of average mixing with the employed chip and conditions.
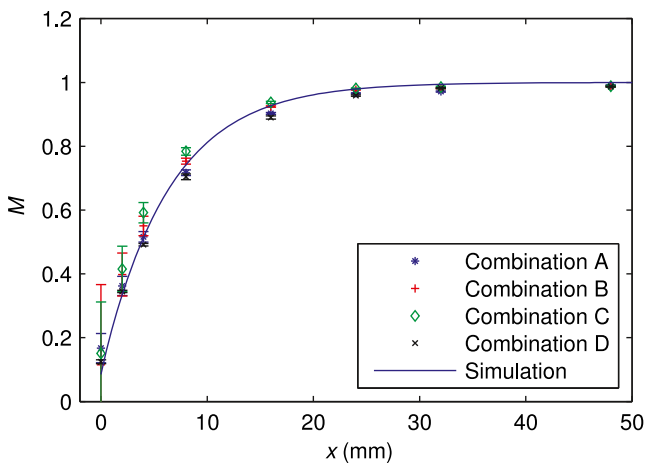
Fig. 8 Diffusive mixing index M, Eq. (3), at a total flow rate 1.0 μL min^{-1} in a channel of 400×150 μm^2 cross section. Combinations A to D measure different combinations of pulsating peristaltic actuation and steady state syringe pump actuation (cf. ESI Fig. 3). Each data point is based on three independent time lapse series, and errorbars indicate the standard deviation between measurements. Simulation results are based on a 2D steady state FEM convection-diffusion model. A diffusion coefficient D of 6×10^{-10} m^2 s^{-1} was employed in the numerical model

3.5 Operability of the system

Assembly of the system takes place in a sterile condition of a LAF bench. The cells were introduced into the chips by loading a cell suspension into the embedded wells in the OCLB and sucking them in by reversing the pump direction. Due to the immediate vicinity to the culture chip combined with a vertical design, the cell loading wells eliminated the risk of cell loading failure due to unwanted upstream sedimentation before loading as can be experienced by for example loading from syringe pumps. Rapid input of cells in the system and increasing the viscosity of cell culture medium by the addition of collagen enhanced uniform plating densities along the chamber length.

Bubble formation and accumulation in the system was initially a serious problem for the low-permeable PMMA chips (unpublished results). This was solved by coupling the inlet and outlet reservoir caps with PTFE tubing and pressurizing the system with air supplemented with 5% CO_2 at 0.3 bar. After pressurizing the system, no air bubbles have been observed even for long perfusion times (3 weeks, unpublished results). In addition, the 5% CO_2 gas mixture improved maintenance of internal gas composition and thus pH of the medium. Since we observed no bubbles in pressurized systems, the need for on-chip bubble traps was eliminated, which eased initial chip filling, simplified chip design and manufacture and permits a greater number of other features, e.g. reaction chambers, to be incorporated within the area of the microfluidic chip.

3.6 Gene expression regulated by pump switching

The doubling time for the HeLa Tet-On® cells in the system was 32.5 h and in good correspondence with previously reported values for growth in conventional dish culture of unmodified HeLa cells and other microfludic systemes (Petronis et al. 2006; Stangegaard et al. 2006). Figure 9 shows an example of the HeLa cells in one of the chambers 24 h after initial seeding.

We used the pTRE-Cycle2 tetracycline and Shield1 regulated gene expression system from Clontech to demonstrate the ability of the microfluidic system to temporally regulate gene expression by external actuation. HeLa Tet-On Advanced cells were cultured and transfected with pTRE-Cycle2-ZsGreen1-DR on chip. Gene expression of mCherry and DD-ZsGreen1-DR was induced by culturing in medium supplemented with doxycycline 0.5 μg mL^{-1}. Regulated gene expression of DD-ZsGreen1-DR was demonstrated by switching to medium with or without 0.5 μM Shield1 in addition to doxycycline. As shown in Fig. 10, the fluorescent signal from DD-ZsGreen1-DR gene expression increased after switching to medium with Shield1 (turning on DD-ZsGreen1-DR gene expression) at approximately the same rate until it stabilized at about 19–21 h. After switching back to medium without Shield1 (turning OFF DD-ZsGreen1-DR gene expression), DD-ZsGreen1-DR was quickly degraded with a half-life of about 4.5 h. These kinetics were similar to DD-YFP expression in NIH3T3 cells (Banaszynski et al. 2006).

4 Discussion

4.1 System

The system was designed for usability and integration with microscopy. The basic design of the presented system comes from the library of components previously presented (Sabourin et al. 2010b). However, in addition to previously presented
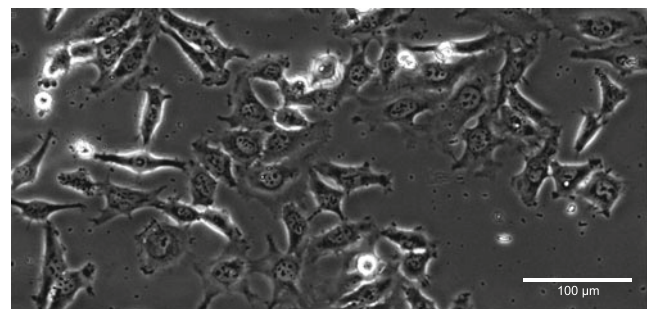

Fig. 9 Phase contrast micrograph at 10× magnification of HeLa cells 24 h after seeding to demonstrate the possibility for phase contrast imaging in the system
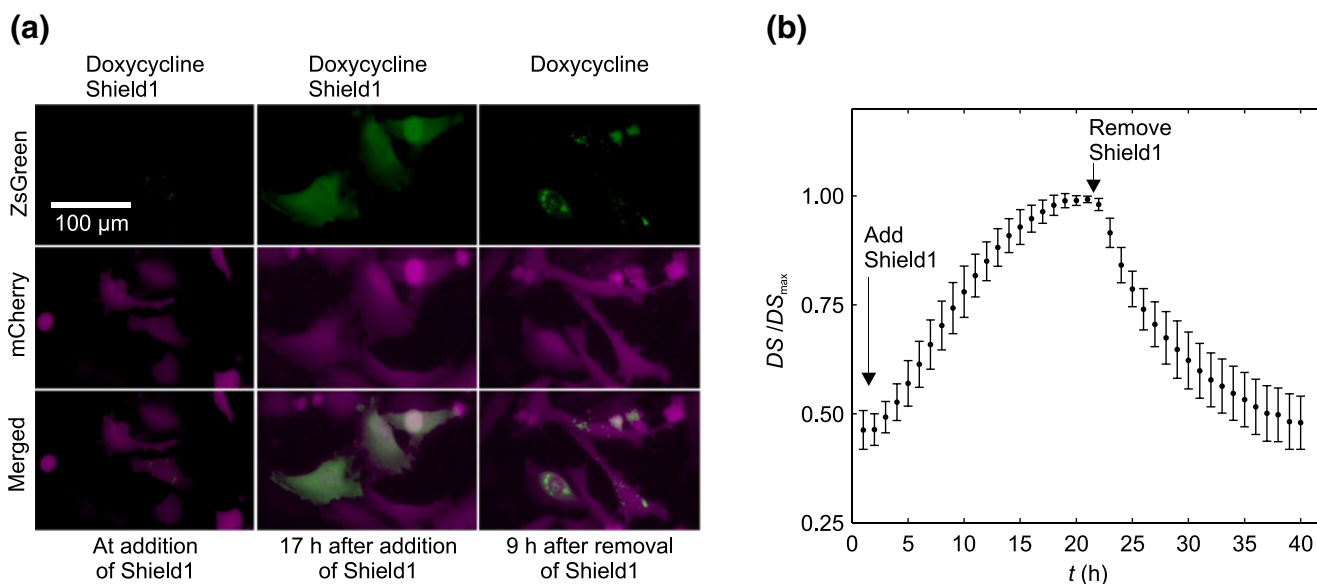
(a)

(b)

Fig. 10 (a) DD-ZsGreen1-DR gene expression was increased (turned ON) by switching to medium added Shield1 and decreased again (turned OFF) by switching to medium without Shield1. Doxycycline induces gene expression of both DD-ZsGreen1-DR and mCherry, but Shield1 regulates DD-ZsGreen1-DR at the protein level by protecting DD-ZsGreen1-DR from degradation. Annotations above micrographs indicate compound composition and annotation below indicate time line. (b) Fluorescent signal of DD-ZsGreen1-DR gene expression plotted against time. Time points for switching to medium with Shield1 and later switching to medium without Shield1 are indicated with arrows. The fluorescent signal measurements are based on the densitometric sum (DS) of individual pixel values. Normalized by highest value (DS_{max}). Error bars indicate standard error of the mean based on six independent cell culture chambers in one experiment

single functional components (Sabourin et al. 2010a; Skafte-Pedersen et al. 2009), this paper demonstrates how the interplay between improved versions of these components combined with application specific microfluidic chips leads to the creation of a robust system capable of performing biological assays with options of parallelization and automation. An example of such assays is the demonstrated real-time gene expression regulation controlled by the system.

Much of the usability of the system is due to the modularity of the individual components and how they are interfaced to the chip. A prime example is the formation of all the 32 interconnections between the systems and the chip by tightening four screws. A second advantage of the system is its portability, particularly between incubators, flow benches and microscope. This is enabled by incorporation of pumps, chips, and vials on common base plates. The only connections to the plate that is needed for operation is a single electrical cable equipped with a standard multi-pin connector and a Luer-Lok pressure connector. As the pumps function as valves when stopped the system can be decoupled from power and pressure and individual reservoirs changed in a LAF bench during long-term experiments, e.g. to limit degradation of fragile compounds with minimal interruption of constant perfusion assays. Due to the self-contained structure, risk of contamination during transport is furthermore minimized and the handling of the system is compatible with existing cell lab work routines and restrictions.

The modular approach for assembly of the system makes it possible to exchange a wide variety of the individual system components with the aid of a screw driver and without having to rebuild the entire system due to contamination, wear or failure of single components. This enhances yield and general usability of the system.

As the system is designed for automated long term cell culture with real-time microscopy it is important to ensure a stable environmental condition. The system itself only ensures control of the fluidic and thus biochemical near-cell conditions and therefore thermal and atmospheric control has to be established by other means. It has previously been demonstrated that on-chip thermal control can be utilized for stand-alone transmission microscopy of long term cell culture (Petronis et al. 2006; Stangegaard et al. 2006). Despite the advantages in terms of portability and demands on external equipment this feature, however, requires on-chip integration of the thermal components, which complicates fabrication, raises the costs of the culturing chips and can give unwanted optical problems such as autofluorescence or shadings. To minimize complexity and cost of the microfluidic system we employed a microscope mounted incubator (Incubator XL Dark S1, Carl Zeiss, Germany), which also ensures thermal stabilization of the microscope. This added feature is especially beneficial for limitation of focus drift over time.

The software is based on VBA and predefined settings for controlling pumps are made in Excel sheets. This

ensures an interface familiar to most users, reduces the requirements on programming skills and facilitates repetition of entire experiments simply by reloading the file. The simple software version decouples the fluidic actuation from the microscope and gives a more flexible, albeit manual, control of the system. Furthermore, it allows the system to be run from most Windows based computers making it suitable for portable applications and work in LAF benches.

4.2 Chips

The microfluidic chips contain only passive microfluidic networks and conform to the standard microscope slide format for easy integration with existing scanners, spotters and other slide handling equipment. Any fluidic control in terms of switching and pumping is handled by the three pumps which are immediately adjacent and in contact with the chip thus minimizing compliance problems. The volume displacement controlled pumping mechanism eliminates the requirements for balanced hydraulic resistance as is necessary for pressure controlled parallel flow systems. This eases the design of chips significantly and allows for rapid prototyping, e.g. with micromilling. The presented setup accommodates for a plethora of chip designs as long as the footprint and interconnections comply with the specified standard. Due to the non-specific mechanical attachment of PDMS interconnections the chip can be made of a variety of materials including, but not limited to, glass, silicon and thermoplastics. The micromilling based chip fabrication scheme used in this paper enables simple fabrication of multilayered, three-dimensional microfluidic networks allowing parallel, serial and combinatorial layouts. For chip fabrication on a larger scale, methods such as injection molding could be considered as an alternative method to produce the individual chip layers.

The chip employed for programmable gene expression distinguishes itself by both allowing for the demonstrated binary on/off situation from each of the inlets as well as a continuous spectrum of mixture ratios. This is possible because the peristaltic pumps both can act as valves and independently control flow rate. The speed of the respective pump is set in the Excel sheet and mixtures of two liquids can easily be established on chip. Depending on the application all three inlets can contain stimulants to be added in varied ratios. However, letting one of the inlets contain a buffer solute the system is readily converted into eight parallel temporal concentration gradient generators each with two stimulants and one diluter. By a proper control of the pumps the overall fluid dynamics near the cells can be maintained through a constant average flow rate while the concentration is varied through the flow rate ratio of the inlets.

4.3 Fluidic control for biological assays

Results on the externally actuated fluidic control showed that the time for switching from one liquid to another in the chip was between seconds to a few minutes (Table 1). The speed of exchanging a liquid from one to another is dependent on the flow velocity at the merging point and diffusion coefficient of the compounds. The flow velocity at the merging point can be increased by employing even smaller channels fabricated with other methods and set the pumps to run at maximum speed (volumetric flow rate 5 μL min^{-1}). It should be noticed that the leak ratio is measured in close proximity to the intersection and thus the downstream response, e.g. in a downstream cell culture chamber as in the design shown in chips such as those presented in Fig. 3(a), will have a natural delay due to channel residence time. The analytical estimate of lag in switch time after long-term stagnancy also shows time scales in the minute range, depending on channel geometry and flow rate. The switching performance compared to the presented results is thus not expected to be significantly reduced even after stagnancy periods on the order of days.

The pumps have a pulsatile flow pattern, which could be of concern for the on-chip fluid dynamics. However, for the employed chips and applications a comparison of models and experiments showed that for both switching and mixing, simple steady-state flow models can be used for design guidelines despite the actual peristaltic actuation. This suggests that the construction of similar systems can be based on corresponding steady-state modeling.

The time to switch one liquid for another with an acceptable contamination ratio is significantly shorter than the typical biological time scale of the presented assays. This has been demonstrated using on-chip transfected HeLa Tet-On cells where the microfluidic system is capable of controlling on-chip gene expression of mCherry and DD-ZsGreen-1-DR by externally mounted pumps. The good temporal correlation between change of pump settings and alteration of gene expression shows that the microfluidic system under the given culture conditions have a response that is sufficiently fast to resolve the time scale of the employed gene expression. The reversibility of the expression also demonstrates that the approach of passive microfluidic chips is a viable tool for this type of assays in that the diffusive leak as expected from the theoretical predictions is insignificant. This means that the use of integrated and more complex approaches is not necessary for these assays, and the experiments can be performed with high cost efficiency on passive, single-use chips.

Based on models and experiments we can thus conclude that passive on-chip networks for switching are performing satisfactory for such biological assays. The time scale of the gene expression in this experiment, which is also typical for

biological processes such as differentiation, cell division, metabolic response and migration, is longer than the fluidic switch time suggesting that the system can be used for a large variety of experiments.

Finally, the presented gene expression results are obtained by fully automated time lapse and the relatively small variation between the individual cultures demonstrate the power of multiple parallel microfluidic channels for gaining data for statistical analysis in a time and cost efficient manner.

4.4 Applications

The presented system is compatible with numerous biological applications. The particular application is tightly connected to the design of the chip attached to the system and the fact that the systems has three motors each controlling eight flow lines simultaneously. One configuration involves 24 chambers on the chip, where each chamber is controlled by one flow line. In such a configuration, it is possible to have well-controlled treatment of cells. Such configuration would for instance support research with the goal to understand signaling pathways involving a soluble compound released from cells or the impact of flow induced stress on the cell. These assays are now being performed in the system for investigation of stem cell differentiation (Hemmingsen et al. 2011), and examples of differentiating cells can be found in ESI Fig. 5 and ESI Fig. 6. In a 24 chamber configuration, it is not possible to obtain automated switching between factors, since the addition of factors to the cells is determined by what is added to the input vials. For temporal control, the system and chip must support feeding in factors to the growth medium over time. As demonstrated in Fig. 10 using the chip shown in Fig. 3(a), the system can support eight independent tests in parallel for temporal investigations. While the experiments shown are based on ZsGreen expression, it is possible to temporally control expression of any gene of interest cloned into a correct expression vector, in this case responding to the presence of doxycycline. Each test site (chamber) can be exposed to two different gradients simultaneously meaning that timely controlled expression of a gene (as driven by doxycycline concentration) can be combined with timely controlled presence of a soluble like cytokine. Due to the coupled actuation of channels by the three pumps, the number of different compounds that can automatically be added per chamber is in the present configuration limited to a maximum of three different compounds. For each chamber, however, these compounds can be unique and need not to be identical with compounds addressing neighboring chambers. Moreover, an expansion of the number of possible compounds can be implemented by adding compatible components capable of routing multiple inlets to the chambers (Conde et al. 2011).While the system is designed and

validated for experiments involving higher eukaryotic cells, the system is not limited to such assays. For instance, we have validated that biochemical assays like DNA microarray analysis are supported by systems using the same components (data not shown). The presented system therefore would support research of for instance hybridization kinetics. Such analysis would increase the understanding of hybridization to and from immobilized probes.

5 Conclusions

We have devised and characterized a cell culture system based on peristaltic micropumps and passive polymeric microfluidic chips. The system allows for easy handling, loading, culturing and stimulation of cells with real-time optical detection. All handling can be performed without skills in micromechanics and components in contact with compounds and cells can be reused or discarded at a low cost through the use of passive microfluidic chips combined with off the shelf reservoirs on a modular system base. The portability and standardized construction of the system conforms well with established work flows and routines in standard cell culture labs. Biocompatibility and temporally controlled exposure has been demonstrated through programmable gene expression. By combining peristaltic pumping with a pressurized system we have eliminated the need for bubble traps in a low-permeable PMMA chip while retaining the advantages of a volume controlled pumping mechanism. The use of PMMA chips with a well defined geometry enables high-quality microscopy with various contrast and fluorescence techniques and ensures a low-permeable culturing surface amenable to coating.

References

H. Andersson, A. van den Berg, Lab on a Chip **6**, 467–470 (2006)

L.A. Banaszynski, L.-C. Chen, L.A. Maynard-Smith, A.G.L. Ooi, T.J. Wandless, Cell **126**, 995–1004 (2006)

A. Bancaud, G. Wagner, K.D. Dorfman, J.-L. Viovy, Anal. Chem. **77**, 833–839 (2005)

A. Buchenauer, M. Funke, J. Büchs, W. Mokwa, U. Schnakenberg, J. Micromech. Microeng. **19**, 074012 (2009)

A.J. Conde, D. Sabourin, P. Skafte-Pedersen and M. Dufva, Proceedings of the 15th International Conference on Miniaturized Systems for Chemistry and Life Sciences (uTAS2011), 2–6 October 2011, Seattle, Washington, USA, eds. J.P. Landers, A. Herr, D. Juncker, N. Pamme, and J. Bienvenue, (CBMS, 2011) pp. 1621-1623 (2011)

N. Futai, W. Gu, J.W. Song, S. Takayama, Lab on a Chip **6**, 149–154 (2006)

R. Gomez-Sjöberg, A.A. Leyrat, D.M. Pirone, C.S. Chen, S.R. Quake, Anal. Chem. **79**, 8557–8563 (2007)

W. Gu, X. Zhu, N. Futai, B.S. Cho, S. Takayama, PNAS **101**, 15861–15866 (2004)

M. Hemmingsen, P. Skafte-Pedersen, D. Sabourin, R.F. Andersen, A.L. Sørensen, P. Collas and M. Dufva, Proceedings of the 15th International Conference on Miniaturized Systems for Chemistry and Life Sciences (uTAS2011), 2–6 October 2011, Seattle, Washington, USA, eds. J.P. Landers, A. Herr, D. Juncker, N. Pamme, and J. Bienvenue, (CBMS, 2011) pp. 834–836 (2011)

C.-C. Hsieh, S.-B. Huang, D.-B. Shieh, G.-B. Lee, P.-C. Wu, G.-B. Lee, Biomedical Microdevices **11**, 903–913 (2009)

P.J. Hung, P.J. Lee, P. Sabounchi, R. Lin, L.P. Lee, Biotechnol. Bioeng. **89**, 1–8 (2005)

L. Kim, M.D. Vahey, H.-Y. Lee, J. Voldman, Lab on a Chip **6**, 394–406 (2006)

J.Y. Kim, H. Park, K.H. Kwon, J.Y. Park, J.Y. Baek, T.S. Lee, H.R. Song, Y.D. Park, S.H. Lee, Biomedical Microdevices **10**, 11–20 (2008)

K.R. King, S. Wang, D. Irimia, A. Jayaraman, M. Toner, M.L. Yarmush, Lab on a Chip **7**, 77–85 (2006)

Y.-K. Lee, P. Tabeling, C. Shih and C.-M. Ho, Proceedings of the ASME International Mechanical Engineering Congress and Exposition, November 5–10, 2000, Orlando, Florida, USA, pp. 505–511 (2000)

P.J. Lee, N. Ghorashian, T.A. Gaige, P.J. Hung, J. Assoc. Lab. Autom. **12**, 363–367 (2007)

S. Lindström, M. Eriksson, T. Vazin, J. Sandberg, J. Lundeberg, J. Frisén and H. Andersson-Svahn, PLOS ONE 4, -, (2009)

M. Liu and Y.-C. Tai, Biomedical Microdevices, 1–11, (2010)

J. Melin, S.R. Quake, Annu. Rev. Biophys. Biomol. Struct. **36**, 213–231 (2007)

I. Meyvantsson, J.W. Warrick, S. Hayes, A. Skoien, D.J. Beebe, Lab on a Chip **8**, 717–724 (2008)

J.Y. Park, S. Takayama, S.-H. Lee, Integr. Biol. **2**, 229–240 (2010)

S. Petronis, M. Stangegaard, C.B.V. Christensen, M. Dufva, Biotechniques **40**, 368–376 (2006)

J.P. Puccinelli, X. Su, D.J. Beebe, J. Assoc. Lab. Autom. **15**, 25–32 (2010)

S.A. Rani, B. Pitts, P.S. Stewart, Antimicrob. Agents Chemother. **49**, 728–732 (2005)

D. Sabourin, D. Snakenborg, M. Dufva, Microfluidics and Nanofluidics **9**, 87–93 (2010a)

D. Sabourin, P. Skafte-Pedersen, V. Coman, M. Hemmingsen, J. Petersen, J.P. Kutter, J. Emneus, D. Snakenborg and M. Dufva, Proceedings of the 14th International Conference on Miniaturized Systems for Chemistry and Life Sciences (uTAS2010), 3–7 October 2010, Groningen, The Netherlands, eds. S. Verporte, H. Andersson, J. Emneus, and N. Pamme (CBMS, 2010) pp. 166–168 (2010b)

P. Skafte-Pedersen, D. Sabourin, M. Dufva, D. Snakenborg, Lab on a Chip **9**, 3003–3006 (2009)

M. Stangegaard, S. Petronis, A.M. Jørgensen, C.B.V. Christensen, M. Dufva, Lab on a Chip **6**, 1045–1051 (2006)

S. Sugiura, J.-I. Edahiro, K. Kikuchi, K. Sumaru, T. Kanamori, Biotechnol. Bioeng. **100**, 1156–1165 (2008)

R.J. Taylor, D. Falconnet, A. Niemistö, S.A. Ramsey, S. Prinz, I. Shmulevich, T. Galitski, C.L. Hansen, Proc. Natl. Acad. Sci. **106**, 3758–3763 (2009)

R. Truckenmüller, P. Henzi, D. Herrmann, V. Saile, W.K. Schomburg, Microsyst. Technol. **10**, 372–374 (2004)

Y.-C. Tung, Y.-S. Torisawa, N. Futai, S. Takayama, Lab on a Chip **7**, 1497–1503 (2007)

G. Velve-Casquillas, M.L. Berre, M. Piel, P.T. Tran, Nano Today **5**, 28–47 (2010)

Z. Wang, M.-C. Kim, M. Marquez, T. Thorsen, Lab on a Chip **7**, 740–745 (2007)

G.M. Whitesides, Lab on a Chip **11**, 191–193 (2011)

M.-H. Wu, S.-B. Huang, G.-B. Lee, Lab on a Chip **10**, 939–956 (2010)

J.H. Yeon, J.-K. Park, Biochip Journal **1**, 17–27 (2007)

E.W.K. Young, D.J. Beebe, Chem. Soc. Rev. **39**, 1036–1048 (2010)

E.W.K. Young, C.A. Simmons, Lab on a Chip **10**, 143–160 (2009)

Z.T.F. Yu, Z.T.F. Yu, K.-I. Kamei, H. Takahashi, X. Wang, G.W. He, C. G. Radu, H.-R. Tseng, Z.T.F. Yu, K.-I. Kamei, G.W. He, R. Silverman, C.G. Radu, O.N. Witte, C.J. Shu, O.N. Witte, O.N. Witte, K.-B. Lee, Biomedical Microdevices **11**, 547–555 (2009)

B. Zhang, M.-C. Kim, T. Thorsen, Z. Wang, Biomedical Microdevices **11**, 1233–1237 (2009)